Appl Phys A (2009) 95: 493–500
DOI 10.1007/s00339-008-4926-z

Applied Physics A
Materials Science & Processing

Network structure and thermal property of a novel high temperature seal glass

M.K. Mahapatra · K. Lu · R.J. Bodnar

Received: 29 September 2008 / Accepted: 1 October 2008 / Published online: 19 October 2008
© Springer-Verlag 2008

Abstract In this study, novel glasses based on SrO–La_2O_3–Al_2O_3–B_2O_3–SiO_2 system are investigated for solid oxide fuel and electrolyzer cells. The network structure evolution of the glasses with increasing B_2O_3:SiO_2 ratio was studied using Raman spectroscopy. The thermal properties of the glasses, including glass transition temperature T_g and glass softening temperature T_d, were studied using dilatometry. The thermal stability of the glasses was investigated using X-ray diffraction. The study shows that as the B_2O_3:SiO_2 ratio increases, the SrO–La_2O_3–Al_2O_3–B_2O_3–SiO_2 glass micro-heterogeneity and the amount of non-bridging oxygen atoms increase. Correspondingly, the T_g of the SrO–La_2O_3–Al_2O_3–B_2O_3–SiO_2 glasses changes from 635 to 775°C, and the T_d changes from 670 to 815°C. Glass thermal stability decreases with B_2O_3:SiO_2 ratio increase. The glass without B_2O_3 is thermally stable after being kept at 850°C for 200 hrs.

PACS 33.20.Fb · 61.05.Cp · 68.60.Dv · 64.70.Ph

M.K. Mahapatra · K. Lu (✉)
Department of Materials Science and Engineering, Virginia Polytechnic Institute and State University, Blacksburg, VA 24061, USA
e-mail: klu@vt.edu
Fax: +1-540-2318919

M.K. Mahapatra
e-mail: mkmanoj@vt.edu

R.J. Bodnar
Department of Geosciences, Virginia Polytechnic Institute and State University, Blacksburg, VA 24061, USA
e-mail: rjb@vt.edu

1 Introduction

Glass is the most preferred candidate as planar solid oxide fuel and electrolyzer cell seals [1]. To be used as a seal, glass should meet a combination of several requirements. Glass transition temperature T_g should be less than cell operating temperature, such as 800°C. Glass softening temperature should be reasonably low (∼800–1000°C) so that glass can bond well with other cell components and will not flow during cell operation. The coefficient of thermal expansion (CTE) of glass should be greater than 9.0×10^{-6}/°C to match with the CTEs of other cell components, which includes yttria-stabilized zirconia, metallic interconnects, and lanthanum manganite. Glass should also be able to sustain stringent reducing and oxidizing environments and not devitrify at solid oxide cell operating temperature for a long time (>50,000 h). Instead of improving mechanical properties, formation of different devitrified phases promotes crack formation due to thermal stress arising from the difference in CTE of the devitrified phases. In addition, glass should wet other cell components but not react severely with them in order to achieve good bonding during operation of cells. Lastly, glass seals must be electrically insulating [2].

BaO containing aluminoboro silicate glass is the most common seal glass due to its excellent thermal properties. However, there are two major drawbacks for this system. First, it crystallizes at 800°C forming celsian ($BaAl_2Si_2O_8$) and its polymorph hexacelcian phases. Both these phases have low CTEs. Also, the difference in CTE values of the celsian phase (2.29×10^{-6}/°C) and the hexacelcian phase (8.0×10^{-6}/°C) develops thermal stress and degrades cell performances [3]. Second, the glasses based on this system interact severely with chromium containing steel interconnect and other fuel cell components [4]. The most detrimental reaction product is $BaCrO_4$, which has a thermal expan-

sion coefficient of 22×10^{-6}/°C. Poor thermal and chemical stabilities of the BaO glass system prompt the need to search for new BaO-free glass systems.

A new glass system based on SrO–La_2O_3–Al_2O_3–B_2O_3–SiO_2 (SABS) has been reported to possess excellent thermal properties [5]. However, La_2O_3 and B_2O_3 degrade the thermal stability of the SABS glass system and contribute to devitrification by forming $LaBO_3$ [6, 7]. Also, B_2O_3 may evaporate in the form of volatile HBO_2 and $B(OH)_3$ species in the presence of water steam at cell operating temperature [8, 9]. There is a need to understand the SABS glass at the network structure level in order to improve the thermal properties of the glass system.

This study is focused on understanding the relations between the network structure and thermal properties of the SABS glass system. To examine the network structural evolution with B_2O_3:SiO_2 ratio change, Raman spectroscopy analysis was carried out. To evaluate the thermal properties of the glasses, including glass transition temperature T_g and glass softening temperature T_d, dilatometry study was employed. To understand the glass thermal stability, X-ray diffraction (XRD) analysis was used.

2 Experimental procedure

2.1 Glass preparation

SABS based glass samples were prepared with the conventional quenching method. $SrCO_3$ (99.9%, Sigma Aldrich, St. Louis, MO), La_2O_3 (99.98%), Al_2O_3 (99.95%), B_2O_3 (99.98%), SiO_2 (99.8%) (all oxides were from Alfa Aesar, Ward Hill, MA) at designed ratios were mixed in a ball mill for overnight. The mixed powders were heated in a platinum crucible in a box furnace (Lindberg, Model No. 51314, Watertown, WI) to 1100°C and kept there for 1 hr for $SrCO_3$ to decompose. After that, the mixture was heated to 1400°C for 4 hrs. The heating rate was 10°C/min. The molten glass was quenched into a graphite mold.

All the glass compositions had 40 mol% of SrO, La_2O_3, and Al_2O_3 at fixed SrO:La_2O_3:Al_2O_3 ratios. The total amount of B_2O_3 and SiO_2 was 60 mol%. The B_2O_3:SiO_2 ratio was varied from 1.4 to 0. The compositions are abbreviated as SABS-0, SABS-5, SABS-10, SABS-15, and SABS-35 in this study. The numbers represent the molar percent of B_2O_3 in each glass composition. Formation of glass phases after quenching was confirmed by XRD study.

2.2 Raman spectroscopy

For network structure analysis of the SABS glass compositions, quenched glass samples were polished to optical finish. Raman spectra of the polished samples were collected in 200–1600 cm^{-1} wave number range using a Raman spectrometer (JY Horbia LabRam HR 800, Horiba Ltd., Japan) with a CCD detector and a Labspec software package. The light source was a 514.57 nm argon laser at 50 mW power and 400 s exposure time. The spectra were later corrected for background noise and temperature effect [10]. For data analysis, the Raman spectra were fitted to Gaussian bands without any restrictions to deconvolute the superimposed Raman peaks [11, 12]. Curve fitting was done with GRAMS/AI (7.02) software (Themo Fisher Scientific, Inc. Waltham, MA).

2.3 Thermal property measurement

Glass transition temperature T_g and dilatometric softening temperature T_d were measured with a push-rod dilatometer (Model 1600R, The Edward Orton Jr. Ceramic Foundation, OH). Cylindrical samples of 27 mm long and 5 mm diameter were used [7]. During the dilatometry study, the samples were heated at 3°C/min heating rate to 900°C for 2 hrs and then cooled to room temperature at the same rate. Each sample was thermally cycled three times under this condition. Average T_g and T_d values were obtained from both the heating and the cooling cycles.

2.4 Phase analysis

For thermal stability study, bulk SABS glass samples were put on a platinum foil and heated to 850°C at the same heating and cooling rate of 5°C/min. The samples were thermally treated at 850°C for 50–200 hrs. XRD studies were carried out in an X'Pert PRO diffractometer (PANalytical B.V., EA Almelo, The Netherlands) to identify the crystalline phases in the thermally treated samples. The scan rate was 0.0020°/s with CuK_α radiation ($\lambda = 1.5406$ Å) and a nickel filter.

3 Results and discussion

3.1 Glass network structure

Thermal properties of a glass depend on the presence of network level structural units, their relative arrangement, and the amounts of bridging and non-bridging oxygen atoms [13]. This is because these structural parameters determine the glass network connectivity. To understand the bonding structure of the SABS glasses, Raman spectroscopy results are shown in Fig. 1.

The Raman spectra of the SABS glasses can be first examined in a general term. In high wave number region (1300–1600 cm^{-1}), the structural units detected are only

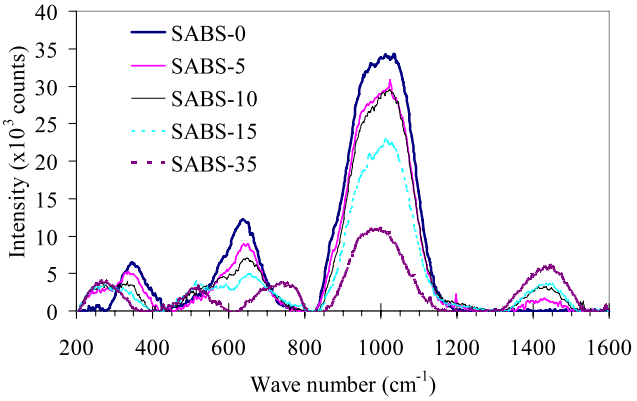

Fig. 1 As collected Raman spectra of different SABS glasses

from B_2O_3 [11]. Both peak width and intensity increase with B_2O_3 content. The peak width increase means decreased local ordering of the B_2O_3-related structural units. The peak intensity increase means that the relative percent of the B_2O_3-related structural units increases. In 800–1200 cm^{-1} wave number region, the spectra contain both B_2O_3 and SiO_2 structural units; the intensity and width of the Raman peaks decrease as the B_2O_3 content increases. The decreased peak width indicates increased local ordering of the B_2O_3-related and the SiO_2-related structural units with B_2O_3 content. The decreased peak intensity means that the relative percent of the B_2O_3-related structural units and the SiO_2-related structural units decreases. In 400–800 cm^{-1} wave number region, the spectra contain both B_2O_3 and SiO_2 structural units; the peak width increases but the peak intensity decreases with B_2O_3 content. This indicates that the B_2O_3 and SiO_2 structural units in this region have less local ordering and the relative percents of the B_2O_3-related structural units and the SiO_2-related structural units decrease. In this region, a tendency of peak splitting is also seen with increasing B_2O_3 content. In lower than 400 cm^{-1} wave number range, the vibration modes are due to complicated twisting and torsion of the silicate networks and motion of the modifier cations. In vitreous silica, continuum is observed below 400 cm^{-1} wave number region [14]. In the SABS glass, distinct peaks are observed. This is believed to be caused by random distribution of tetrahedral structural units and Si–O–Si bond angles, as well as the structural units from the glass modifiers SrO and La_2O_3 [15]. The peaks shift to lower wave numbers as B_2O_3 content increases, indicating the increasing effect of the modifier species on the SABS glass network structure. However, detailed data on the bonding characteristics between the glass formers (SiO_2 and B_2O_3) and glass modifiers (SrO and La_2O_3) are beyond the scope of the current study.

To analyze the network structure of the SABS glasses, it is beneficial to examine silicate glass and borate glass structures first. In silicate glass, there are four major peaks representing the nature and contribution of different silicate structural units. The 1050–1100 cm^{-1} region describes the stretching motion of disilicate composition with three bridging oxygen atoms. The 950–1000 cm^{-1} peak describes the stretching motion of metasilicate composition with two bridging oxygen atoms. The 900 cm^{-1} peak reflects the pyrosilicate composition with one bridging oxygen atom. The 850 cm^{-1} peak represents orthosilicate composition with zero bridging oxygen atoms [16]. In this context, the silicate units with four bridging oxygen atoms, three bridging oxygen atoms, two bridging oxygen atoms, one bridging oxygen atom, and zero bridging oxygen atom can be denoted as Q^4, Q^3, Q^2, Q^1, and Q^0, respectively. The 400–700 cm^{-1} peak is due to the delocalized vibration of Si–O–Si bonding from mixed stretching and bending modes [17]. In borate glass, the 1300–1600 cm^{-1} peak describes the $B–O^-$ (O^- denotes the non-bridging oxygen) stretching mode with chain and ring metaborates which also connect the network [18]. Based on the above understanding, peaks in different wave number ranges of the SABS glass spectra can be identified. However, individual peaks corresponding to different structural units have a tendency to overlap due to a high degree of disorder (peak widening). Also, wave number peak shift occurs for such complex glass systems [13, 14]. To establish the correlation between the Raman peaks and specific glass structural units, the spectrum for each SABS glass sample needs to be deconvoluted. The deconvoluted spectra for different SABS glass compositions in the 400–1600 cm^{-1} range are given in Fig. 2. With the understanding that the composition difference between the conventional silicate glass and the SABS glasses can cause some peak shift, individual de-convoluted peaks can be identified. In this study, detailed Raman spectrum analysis can be separated into three wave number regions: 1200–1600 cm^{-1}, 800–1200 cm^{-1}, and 400–800 cm^{-1}, as outlined previously.

For the SABS-0 glass, no peaks are detected in the 1300–1600 cm^{-1} wave number range, corresponding to the Raman peaks from B_2O_3. This is easy to understand because the SABS-0 glass is B_2O_3 free. For the SABS-5 and SABS-10 glasses, the 1426 cm^{-1} peak is identified to be from the metaborate units [19]. For the SABS-15 glass, multiple peaks are identified after Raman peak deconvolution. The presence of 1387 and 1357 cm^{-1} peaks indicates the $B–O^-$ vibrations in a large borate network [18]. The peaks at 1424, 1452, 1460, 1479, and 1501 cm^{-1} can be assigned to the metaborate units and localized stretching vibration modes of $B–O^-$ bonds as for the 1426 cm^{-1} peak in the SABS-5 and SABS-10 glasses. The two peaks at 1402 and 1438 cm^{-1} cannot be identified. In the SABS-35 glass, the peaks at 1354, 1382, and 1394 cm^{-1} can be assigned to the splitted 1380 cm^{-1} peak identified for the $B–O^-$ vibrations [18].

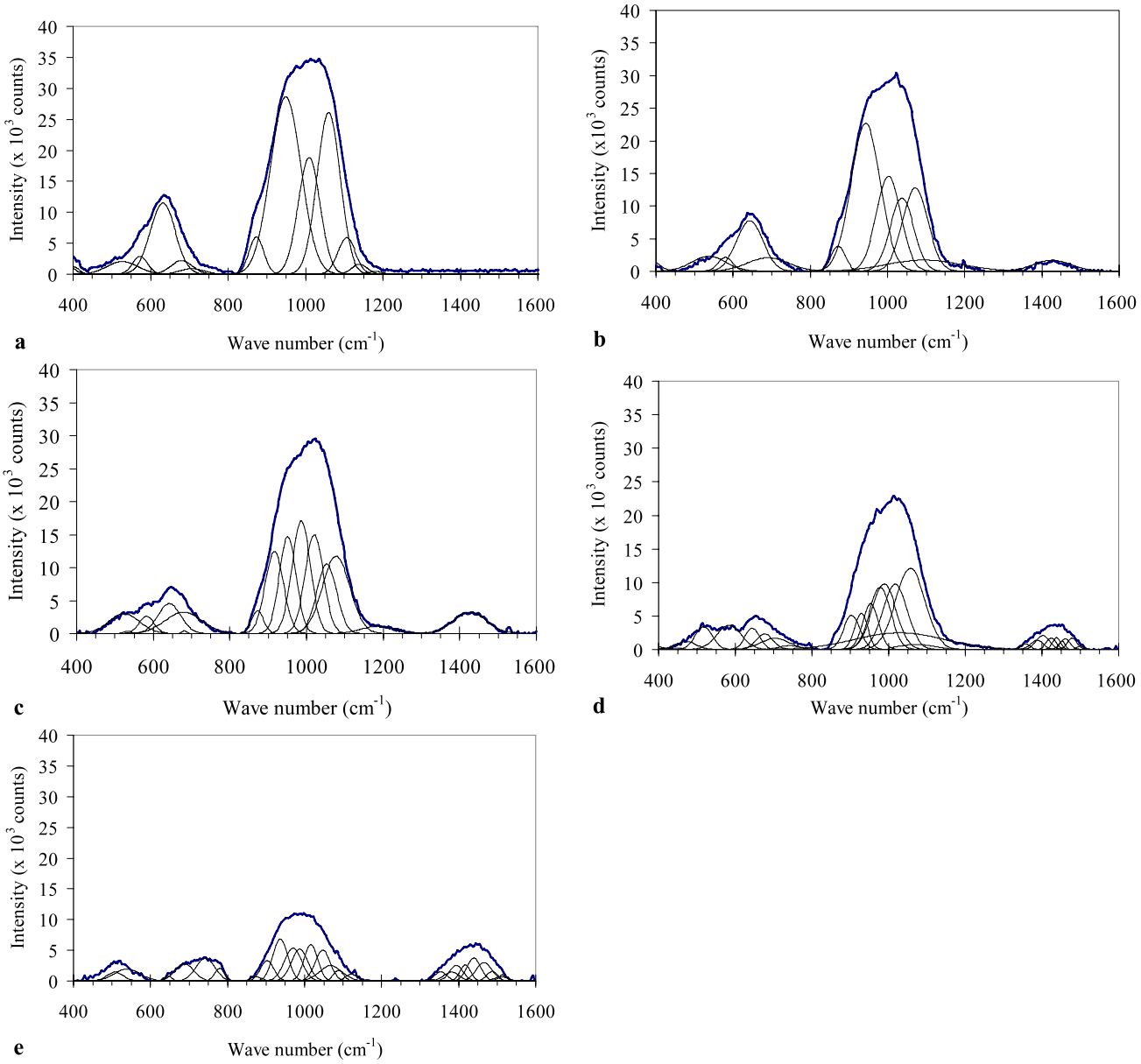

Fig. 2 Deconvoluted Raman spectra for: (**a**) SABS-0, (**b**) SABS-5, (**c**) SABS-10, (**d**) SABS-15, and (**e**) SABS-35 glasses

The peaks at 1466, 1487, 1510, and 1514 cm^{-1} can be assigned to localized stretching vibration of the B–O^- bonds which would be at 1468, 1475, and 1490 cm^{-1} wave numbers [10, 17]. The 1330, 1417, and 1443 cm^{-1} peaks cannot be identified. Also, the high wave number Raman peak intensity increases with B_2O_3 content increase. From this analysis, it can be concluded that B_2O_3 progressively participates in the SABS network structure [17]; the relative amount of non-bridging oxygen atoms increases and the glass network becomes less connected with B_2O_3 content increase.

For the de-convoluted peaks in the 800–1200 cm^{-1} wave number range, it can be understood as follows. For the SABS-0 glass, the weak 1180 and 1143 cm^{-1} peaks correspond to the splitted 1060–1200 cm^{-1} peak in vitreous silica when peak shifting is considered [20]. These peaks describe the four bridging oxygen atom Q^4 units. The 1060 and 1105 cm^{-1} peaks are from the three bridging oxygen atom Q^3 units. The 1010 and 949 cm^{-1} peaks are from the two bridging oxygen atom Q^2 units. The 872 cm^{-1} peak is from the Q^0 units. For the SABS-5 glass, no Q^4 glass network units are detected. The 1037, 1072, and 1094 cm^{-1} peaks are from the Q^3 units. The 943 and 1003 cm^{-1} peaks are from the Q^2 units. The 872 cm^{-1} peak is from the Q^0 units. In the SABS-10 glass, the peak at 1188 cm^{-1} is from the diborate or pyroborate units [18]. The peaks at 1053 and

1077 cm^{-1} are from the Q^3 units. The peaks at 951, 986, and 1020 cm^{-1} are from the Q^2 units. The peak at 916 cm^{-1} is from the Q^1 units. The 872 cm^{-1} peak is from the Q^0 units. For the SABS-15 glass, the 1056 cm^{-1} peak is from the Q^3 units. The 953–1028 cm^{-1} peaks are from the Q^2 units. The 929 cm^{-1} peak is from the $Si(OAl)_3$ units with one bridging oxygen atom [21]. The 904 cm^{-1} peak is from the Q^1 units. For the SABS-35 glass, the 1122 cm^{-1} peak is attributed to the diborate units. The 1068 and 1089 cm^{-1} peaks are attributed to the Q^3 units. The 970–1047 cm^{-1} peaks are attributed to the Q^2 units. The 937 cm^{-1} peak represents orthoborate or B–O–Si stretching mode [22]. The 875 and 903 cm^{-1} peaks correspond to the Q^1 and Q^0 units, respectively. This means some B–O–Si bonds exist in the SABS-35 glass. Again, the Raman peak analysis in the 800–1200 cm^{-1} region shows that B_2O_3 content increase causes boron-containing structural unit formation. Also, the amounts of silicon-containing structural units decrease. Both aspects indicate that the SABS glass network connectivity decreases.

For the SABS-0 glass, the 619 and 641 cm^{-1} peaks are from the two bridging oxygen atom Q^2 units corresponding to the characteristic peaks of metasilicate glasses between 620–640 cm^{-1}. The 606 cm^{-1} peak is from the broken Si–O bonds as in vitreous silica with the Q^3 units. For the SABS-5 glass, the 643 cm^{-1} peak is from the Q^2 units. The 690 cm^{-1} peak is from the Q^1 units [17]. The 537 and 580 cm^{-1} peaks are from the $[BO_4]$ units in anionic rings. For the SABS-10 glass, the peaks at 679 and 680 cm^{-1} peaks are from mixed Si–O–B linkage with the Q^1 units. Some metaborate units may also contribute to these peaks. The 642 cm^{-1} peak is from the Q^2 units. Some metaborate units also appear at the 642 cm^{-1} peak since the integral area increases with increasing B_2O_3 content. The peaks at 524, 534, and 582 cm^{-1} are from the BO_4^- anionic rings. For the SABS-15 glass, the 741–744 cm^{-1} peaks are attributed to the BO_4^- tetrahedral units. The 677 and 704 cm^{-1} peaks are attributed to the Q^1 units along with some metaborate units. The peaks in the 400–644 cm^{-1} region are attributed to delocalized vibration of Si–O–Si bridging units. The 644 cm^{-1} peak is from the Q^2 units. The 517 and 583 cm^{-1} peaks are from the BO_4^- units. The 471 cm^{-1} peak is due to the bending mode of B–O–B, B–O–Si, and Si–O–Si linkages associated with the Q^3 units [22]. The 446 cm^{-1} peak is from the Q^4 units. Simultaneous presence of 929 and 471 cm^{-1} peaks indicates B–O–Si linkages. In alkaline borate glass and alkaline earth borate glass, simultaneous presence of 930, 650, and 485 cm^{-1} peaks confirms the presence of pentaborate unit, and the 755 cm^{-1} peak is from dipentaborate units [22]. In the SABS-35 glass, simultaneous presence of 937, 779, 645, and 508 cm^{-1} peaks confirms the presence of pentaborate and dipentaborate structural units. The 742 cm^{-1} peak is attributed to the BO_4^- tetrahedra. The 467 and 688 cm^{-1} peaks are attributed to B–O–Si linkages. The 688 cm^{-1} peak may also be attributed to the metaborate units. The peak at 539 cm^{-1} is attributed to the BO_4^- units. As it shows, peak splitting increases with B_2O_3 content increase. From SABS-0 to SABS-35 glass, the boron-containing structure units change from metaborate to pentaborate and even to dipentaborate with non-bridging oxygen atoms.

With the understanding that Raman spectroscopy can only provide a qualitative picture of the overall glass structure, the following observations can be made: (a) The amount of non-bridging oxygen atoms increases along with the appearance of metaborate, orthoborate, and pentaborate units with increasing B_2O_3 content. B_2O_3 reduces the connectivity of the SABS glass. (b) Peak splitting appears and then increases with increasing B_2O_3 content, suggesting increased local ordering of the structural units in the SABS glasses. (c) The peaks corresponding to B–O–Si linkages indicate that borate groups or boroxol rings mix with SiO_4 tetrahedral structural units.

3.2 Thermal properties

The T_g and T_d results obtained from the dilatometry experiments are shown in Fig. 3. The figure excludes the data of the first heating cycle because the samples used in this experiment were not annealed [7]. From Fig. 3 it is observed that both T_g and T_d decrease as B_2O_3 content increases from 0 to 35 mol%. The T_g value changes from 775 to 635°C. The T_d value changes from 815 to 670°C. This means the SABS glass network connectivity decrease directly affects the thermal properties [23].

The trend in decreased values of T_g and T_d with increasing B_2O_3 content is expected due to the low T_g and T_d of borate glass, contributed by the presence of $[BO_3]$ trigonal structures. The SABS-0 glass consists of stable $[SiO_4]$ tetrahedra in a connected network structure. A small amount

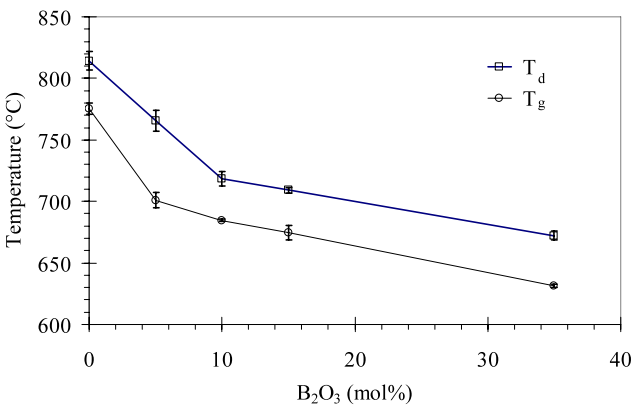

Fig. 3 Glass transition temperature (T_g) and glass softening temperature (T_d) variation with B_2O_3 content in SABS glasses

of the Q^4 units is present along with the Q^3, Q^2, and Q^0 units in the SABS-0 glass. The T_g and T_d are high since the glass network is more rigid and less mobile. As B_2O_3 is introduced into the SABS-5 glass, trigonal [BO_3] polyhedra cause the [SiO_4] glass network to re-arrange and result in a less connected 3D structure. In the SABS-5 glass, the amount of the Q^3 units increases and the amount of the Q^2 units decreases with the appearance of metaborate units and boroxol rings. Due to the presence of metaborate units and trigonal boroxol rings, the degree of connectivity decreases and consequently both T_g and T_d decrease sharply. With increasing B_2O_3 content, the content of the [SiO_4] structural units decreases and the content of the [BO_3] structural units increases. However, with increasing B_2O_3:SiO_2 ratio, the content of the borate structural units with both three and four-coordinated borons (metaborate, pentaborate, and orthoborate) increases. The bond energy of B–O–Si bond with four coordinated boron is 89 kcal/mol compare to 119 kcal/mol for B–O–Si bond with three coordinated boron [24]. The absence of the characteristic peak, 805 cm^{-1}, of boroxol rings with three coordinated boron in the SABS glasses indicates the dominance of the four coordinated borate structural units. The weaker bond energy of four coordinated B–O–Si bond also contributes to the lower T_g and T_d in the SABS glasses with increasing B_2O_3:SiO_2 ratio. In the SABS-15 glass, the amount of the Q^2 units decreases with the evolution of pentaborate units along with more metaborate and boroxol ring units. In the SABS-35 glass, decreased amount of the Q^3 units and increased amount of the pentaborate units further decrease the glass network connectivity, resulting in lower T_g and T_d. As a result, the decrease in T_g and T_d becomes more substantial.

3.3 Thermal stability

Degree of glass network connectivity directly affects the devitrification tendency of a glass system. Decrease in connectivity increases the possibility for devitrification. If structural unit local ordering occurs in a glass, even if only in small localized areas, the glass will be prone to devitrification, likely caused by heterogeneous nucleation [25].

For the SABS-0 glass, the thermal treatment at 850°C is carried out up to 200 hrs. The XRD patterns at different thermal treatment times are given in Fig. 4. As can be seen from the halo shape of the XRD patterns, the glass does not devitrify after 200 hrs of thermal treatment. This result suggests that the SABS-0 glass is very thermally stable.

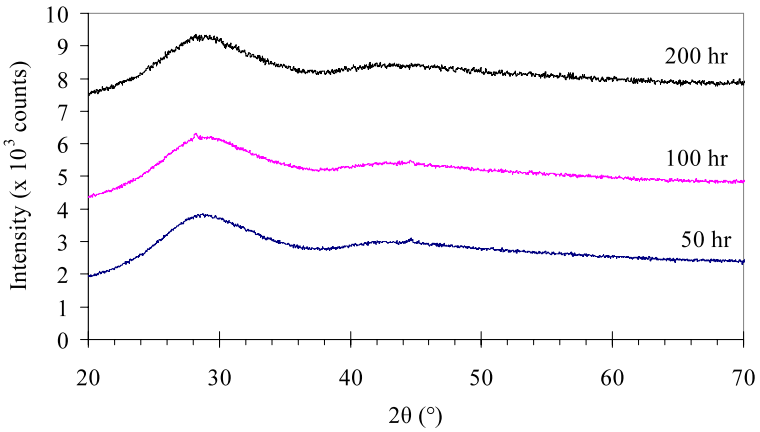

Fig. 4 XRD patterns of SABS-0 glass thermally treated at 850°C for different times

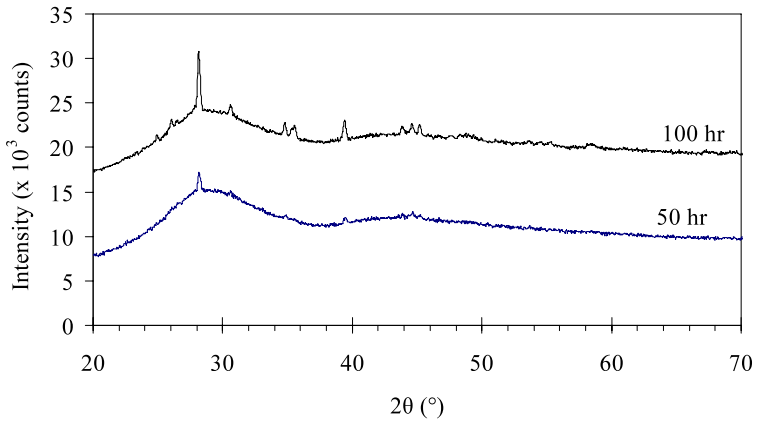

Fig. 5 XRD patterns of SABS-5 glass thermally treated at 850°C for different times

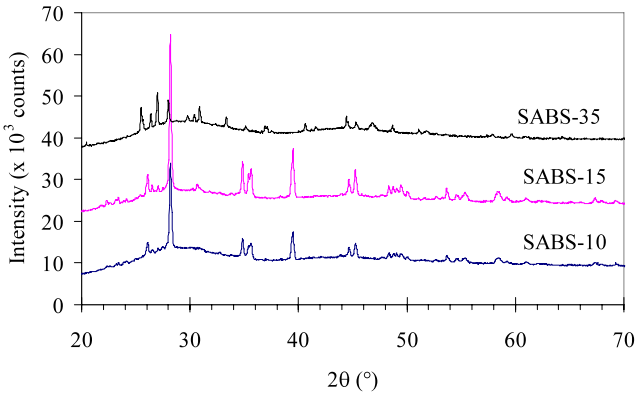

Fig. 6 XRD patterns of SABS-10, SABS-15, and SABS-35 glasses thermally treated at 850°C for 50 hrs

For the SABS-5 glass, thermal treatment was conducted up to 100 hrs at 850°C. The glass devitrifies after 50 hrs of thermal treatment as seen in Fig. 5. Small devitrification peaks are observed, but the intensity and the number of peaks are insufficient to determine the crystalline phases. After 100 hrs of thermal treatment at 850°C, monoclinic $La_2Si_2O_7$ is the main phase along with small amounts of α-$SrSiO_3$ and Sr_2SiO_4 phases. This means as the glass structure connectivity decreases, [SiO_4] becomes more likely to interact with glass modifiers, such as SrO and La_2O_3, and form new species. This interaction away from the glass network leads to devitrification and crystalline phase formation.

The SABS-10, SABS-15, and SABS-35 glasses are thermally treated at 850°C for 50 hrs only since devitrification becomes apparent at this condition, as shown in Fig. 6. Monoclinic lanthanum silicate ($La_2Si_2O_7$) is the only phase in the SABS-10 glass. Three phases are identified in the SABS-15 glass. They are monoclinic lanthanum silicate ($La_2Si_2O_7$), rhombohedral aluminum borate ($AlBO_3$), and orthorhombic strontium boron aluminum oxide ($Sr_2B_2Al_2O_8$). In the SABS-35 glass, two phases, orthorhombic strontium borate (SrB_2O_4) and orthorhombic lanthanum borate ($LaBO_3$), are identified. $LaBO_3$ is the main phase. This appearance of totally different phases in the SABS-35 glass is also seen in the peak shifting in the XRD patterns whereas the major peaks are exactly overlapped for the SABS-10 and the SABS-15 glasses (Fig. 6).

In the studied SABS glass system, only B_2O_3:SiO_2 ratio changes. With increasing B_2O_3 content, different devitrified phases evolve. This indicates that the devitrification process is accompanied by the complex interaction between different glass structural units and glass modifiers. Gibbs free energy change during the devitrification process may be the most convincing approach to explain the devitrification tendency and the most likely devitrifying phases. However, thermodynamic data for the SABS glass system at high temperatures are not available, especially for the species involving SrO and La_2O_3 modifiers. Because of this, structural evolution data obtained from Raman spectroscopy provide the best knowledge about the devitrification tendency of the studied SABS glass systems.

In borosilicate glasses, borate structural units and silicate structural units do not disperse well and tend to stay separated. This glass structural unit clustering is supported by the peak splitting in the deconvoluted Raman spectra in Fig. 2. The amount of non-bridging oxygen atoms increases with B_2O_3 addition. Thus, the amount of glass structural units with low connectivity increases. The presence of localized low connectivity structural units promotes devitrification via nucleation in the glass [26, 27]. Therefore, devitrification is more prominent with increasing B_2O_3:SiO_2 ratio.

Another important aspect to consider for the SABS glass system is the glass modifiers. The non-bridging oxygen atoms tend to coordinate with the glass modifiers and form new species. In K_2O–La_2O_3–SiO_2 system, the non-bridging oxygen atoms due to the Q^3 units at 1030 and 1100 cm^{-1} peaks coordinate with La^{3+} ions [28]. In lanthanum containing glasses, La^{3+} ions either bond with silicate tetrahedra forming 'lanthanide Q^3' species (Si–O–La) or link with other La–O bonds forming La–O–La [29, 30]. These structural units are energetically favorable [31] and form small, isolated, phase-ordered domains which essentially also act as nucleation sites favoring devitrification of glass. In the SABS glasses, La^{3+} and Sr^{2+} ions act as modifiers. The intense peaks in the 1020–1030 cm^{-1} region in the SABS-5 (1037 cm^{-1}), SABS-10 (1020 cm^{-1}), and SABS-15 (1028 cm^{-1}) glasses suggest that the non-bridging oxygen atoms from the Q^3 units coordinate with La^{3+}. Consequently, $La_2Si_2O_7$ phase forms in the SABS-5, SABS-10, and SABS-15 glasses. For the SABS-35 glass, similar argument can be applied. Some non-bridging oxygen atoms are coordinated with Sr^{2+} ions and thus Sr-containing phases evolve. The isolated La–O clusters probably bond with borate structural units and form B–O–La instead of B–O–Si due to the higher concentration of borate structural units and higher electrostatic bond strength of boron (1.62) than silicon (1.54). Consequently, $LaBO_3$ phase forms as the main phase in the SABS-35 glass. This interpretation is also supported by the appearance of several peaks above 1300 cm^{-1} wave number, similar to the crystalline phase $La(B_3O_6)$ peak in BaO–La_2O_3–B_2O_3 metaborate glass [18, 32]. With B_2O_3 content increase in the SABS glasses, the metaborate, orthoborate, pentaborate, and dipentaborate structural units evolve as seen from the Raman spectroscopy results. These borate structural units contain both four-coordinated and three-coordinated boron atoms [33]. In strontium containing boroaluminate glass, devitrification is favored by the interaction of three coordinated boron atoms and four coordinated aluminium atoms, forming boroaluminate phase [34, 35]. With increasing B_2O_3 content, the tetraderal BO_4 structural

units (four-coordinated boron) break the Al–O–Al bonds in the SABS glass network to form Al–O–B bonds and react with $SrAl_2O_4$ to form strontium aluminoborate and strontium borate phases [36]. Consequently, with increasing B_2O_3 content, $AlBO_3$ and $Sr_2B_2Al_2O_8$ phases evolve along with $La_2Si_2O_7$ phase in SABS-15 glass, and SrB_2O_4 evolves along with $LaBO_3$ phase in SABS-35 glass.

4 Conclusions

The effects of B_2O_3 content on the network structure and thermal properties of the SrO–La_2O_3–Al_2O_3–B_2O_3–SiO_2 glass system are studied. Local ordering of the glass structural units and the amount of non-bridging oxygen atoms increase with increasing B_2O_3:SiO_2 ratio. Increased B_2O_3 content also degrades the thermal properties, including glass transition temperature and softening temperature. The micro-heterogeneity from different glass structural units also increases the tendency of devitrification and degrades thermal stability. Boron free SABS glass exhibits excellent combination of thermal properties and thermal stability.

Acknowledgements This material is based upon work supported by the Department of Energy under Award Number DE-FC07-06ID14739. The help of Mr. Charles Farley, Department of Geoscience, Virginia Tech, during Raman spectroscopy experiment is highly appreciated.

References

1. EG & G Technical Services: Fuel Cell Handbook. US Department of Energy, Office of Fossil Energy, National Energy Technological Laboratory, Morgantown, West Virginia (2004)
2. P.A. Lessing, J. Mater. Sci. **42**, 3465 (2007)
3. S.B. Sohn, S.Y. Choi, G.H. Kim, H.S. Song, G.D. Kim, J. Am. Ceram. Soc. **87**, 254 (2004)
4. Z. Yang, G. Xia, K.D. Meinhardt, K.S. Weil, J.W. Stevenson, J. Mater. Eng. Perform. **13**, 327 (2004)
5. K.L. Ley, M. Krumpelt, R. Kumar, J.H. Meiser, I. Bloom, J. Mater. Res. **11**, 1489 (1996)
6. M.K. Mahapatra, C. Story, K. Lu, W.T. Reynolds Jr., in *Energy: Fuel Cells: Materials, Processing, Manufacturing and Power Management Technologies. Proc. Mater. Sci. Tech.*, Detroit, Michigan, USA, 16–20 September 2007, pp. 371–380
7. M.K. Mahapatra, K. Lu, W.T. Reynolds Jr., J. Power Sources **179**, 106 (2008)
8. M.J. Snyder, M.G. Mesko, J.E. Shelby, J. Non-Cryst. Solids **352**, 669 (2006)
9. S.T. Reis, R.K. Brow, T. Zhang, P. Jasinski, Ceram. Eng. Sci. Proc. **27**, 297 (2006)
10. A.K. Hassan, L.M. Torell, L. Börjesson, H. Doweidar, Phys. Rev. B: Condens. Matter Mater. Phys. **45**, 12797 (1992)
11. B.O. Mysen, L.W. Finger, D. Virgo, F.A. Seifert, Am. Mineral. **67**, 686 (1982)
12. H. Li, P. Hrma, J.D. Vienna, M. Qian, Y. Su, D.E. Smith, J. Non-Cryst. Solids **331**, 202 (2003)
13. J.E. Shelby, *Introduction to Glass Science and Technology* (Royal Society of Chemistry, Cambridge, 2005)
14. S.K. Sharma, J.F. Mammone, M.F. Nicol, Nature **292**, 140 (1981)
15. T. Furukawa, W.B. White, J. Non-Cryst. Solids **87**, 38–39 (1980)
16. P. McMillan, Am. Mineral. **69**, 622 (1984)
17. E.I. Kamitsos, J.A. Kapoutsis, H. Jain, C.H. Hsieh, J. Non-Cryst. Solids **171**, 31 (1994)
18. R.K. Brow, D.R. Tallant, G.L. Turner, J. Am. Ceram. Soc. **79**, 2410 (1996)
19. M. Środa, C. Paluszkiewicz, J. Mol. Struct. **302**, 834–836 (2007)
20. F. Seifert, B.O. Mysen, D. Virgo, Am. Miner. **67**, 696 (1982)
21. B.O. Mysen, D. Virgo, F.A. Seifert, Am. Miner. **70**, 88 (1985)
22. B.N. Meera, J. Ramakrishna, J. Non-Cryst. Solids **159**, 1 (1993)
23. J.E. Shelby, J. Appl. Phys. **50**, 8010 (1979)
24. W.F. Du, K. Kuraoka, T. Akai, T. Yazawa, J. Mater. Sci. **35**, 4865 (2000)
25. W. Vogel, *Structure and Crystallization of Glass* (Pergamon, New York, 1971)
26. B.H.W.S.D. Jong, K.D. Keefer, G.E. Brown Jr., C.M. Taylor, Geochim. Cosmochim. Acta **45**, 1291 (1981)
27. J. Deubener, J. Non-Cryst. Solids **351**, 1500 (2005)
28. A.J.G. Ellison, P.C. Hess, J. Non-Cryst. Solids **127**, 247 (1991)
29. M. Wilding, Y. Badyal, A. Navrotsky, J. Non-Cryst. Solids **353**, 4792 (2007)
30. T. Schaller, J.F. Stebbins, M.C. Wilding, J. Non-Cryst. Solids **243**, 146 (1999)
31. M.C. Wilding, A. Navrotsky, J. Non-Cryst. Solids **265**, 238 (2000)
32. I.N. Chakraborty, J.E. Shelby, S. Robert, A. Condrate, J. Am. Ceram. Soc. **67**, 782 (1984)
33. W.J. Dell, P.J. Bray, S.Z. Xiao, J. Non-Cryst. Solids **58**, 1 (1983)
34. B.C. Bunker, R.J. Kirkpatrick, R.K. Brow, J. Am. Ceram. Soc. **74**, 1425 (1991)
35. B.C. Bunker, R.J. Kirkpatrick, R.K. Brow, G.L. Turner, C. Nelson, J. Am. Ceram. Soc. **74**, 1430 (1991)
36. A. Nag, T.R.N. Kutty, J. Alloys Compd. **354**, 221 (2003)